

Electron Heat Transport down Steep Temperature Gradients

J. P. Matte

*Institut Nationale de la Recherche Scientifique-Energie, Université du Québec, Varennes,
Québec J0L2P0, Canada*

and

J. Virmont

*Equipe du GRECO Interaction Laser-Matière, Groupe de Recherche du Centre National de la Recherche
Scientifique, Laboratoire de Physique des Milieux Ionisés, Ecole Polytechnique,
F-91128, Palaiseau, France*

(Received 14 October 1982)

Electron heat transport is studied by numerically solving the Fokker-Planck equation, with a spherical harmonic representation of the distribution function. The first two terms (f_0, f_1) suffice, even in steep temperature gradients. Deviations from the Spitzer-Härm law appear for λ/L_T [(mean free path)/(temperature gradient length)] ≥ 0.01 , as a result of non-Maxwellian f_0 . For $\lambda/L_T \geq 1$, the heat flux is $\frac{1}{3}$ of the free-streaming value. In intermediate cases, a harmonic law describes well the hottest part of the plasma.

PACS numbers: 52.50.Jm, 44.10.+i, 52.25.Fi, 52.65.+z

Laser-plasma interactions are modeled with fluid codes¹ in which heat transfer is described by the Spitzer-Härm² heat diffusion law. However, this law overestimates the heat flux near the critical surface because of the steepness of the temperature gradient,³ and the codes usually limit the heat flux Q to a fraction f of the "free-streaming" value $Q_{FS} = nKT_e(KT_e/m)^{1/2}$.¹ The fact that f needs to be a small number (0.03) to fit experimental data¹ has prompted research into the mechanisms responsible for this "flux inhibition."^{1,3-9} Furthermore, near the ablation front, the Spitzer diffusion law predicts a very small heat flux because of the low temperature, but cannot describe preheat by hot electrons streaming from the corona. Inward heat flow strongly influences the target behavior (ablation, lateral thermal smoothing, etc.).¹ Also, in linear device-

es, such as θ pinches, heat flow at the ends is the main energy-loss mechanism, and any heat-flux inhibition would have important consequences.¹⁰

To obtain more insight into heat transport, it is necessary to solve the electron kinetic equation: the Vlasov equation with Fokker-Planck collision operators to describe both electron-electron and electron-ion collisions. Such a computation may be done either by particle simulation^{4,5} or by an expansion in spherical harmonics.⁶ We have chosen the latter method.

The distribution function is written

$$f(\vec{r}, \vec{v}, t) = \sum_{i=0}^N f_i(x, v, t) P_i(\mu), \quad (1)$$

where $\mu = v_x/v$. The advancement of the f_i 's in time is given by

$$\begin{aligned} \frac{\partial f_l}{\partial x} + v \frac{\partial}{\partial x} \left(\frac{l}{2l-1} f_{l-1} + \frac{l+1}{2l+3} f_{l+1} \right) - \frac{eE}{m} \frac{l}{2l-1} \left(\frac{\partial f_{l-1}}{\partial v} - \frac{l-1}{v} f_{l-1} \right) + \frac{l+1}{2l+3} \left(\frac{\partial f_{l+1}}{\partial v} + (l+2) \frac{f_{l+1}}{v} \right) \\ = - \frac{-D_{\perp} l(l+1)}{2v^2} f_l + \frac{1}{v^2} \frac{\partial}{\partial v} \left[v^2 \left(\frac{D_{\parallel}}{2} \frac{\partial f_l}{\partial v} + C f_l \right) \right], \end{aligned} \quad (2)$$

where E is the self-consistent electric field. $D_{\perp}(v)$, $D_{\parallel}(v)$, and $C(v)$ are, respectively, the coefficients of scattering, parallel diffusion, and friction. They are computed by integration over f_0 , i.e., anisotropy is neglected when computing the collision operators, as in previous work.⁴⁻⁶ Numerical details may be found elsewhere.⁸

In the present work, we have solved the follow-

ing problem: a plasma slab of length L contained between two thermostatic walls at temperatures T_1 and T_2 . The electrons which reach a wall are replaced by a half Maxwellian distribution at the prescribed temperature and at a rate such that the current is cancelled. The ions ($Z=5$) are assumed cold, immobile, and of uniform density

as in previous work.⁴⁻⁷ This problem is conceptually simpler, as it involves only transport, than the problem solved in Refs. 4 and 6, where the temperature gradient is maintained by heating which interacts with transport. In Refs. 5 and 7, thermostatic boundary conditions were used, but we have used larger values of T_1/T_2 and have included the E field and the collisions self-consistently.

The simulations are all initialized by a prescribed temperature profile (from T_1 to T_2) and with the assumption that, everywhere, the electrons are isotropic and Maxwellian. Initially, anisotropic components build up and some electrostatic oscillations are seen, but these quickly damp away (because of collisions). We then see heat flow from the hot to the cold region, and an advancing heat front. This transient state is of physical interest, and will be discussed later. When the heat front reaches the cold wall, we see a steady state with uniform heat flux and time-independent temperature profile. It is this steady-state situation which we have examined most closely, and with the most varied parameters.

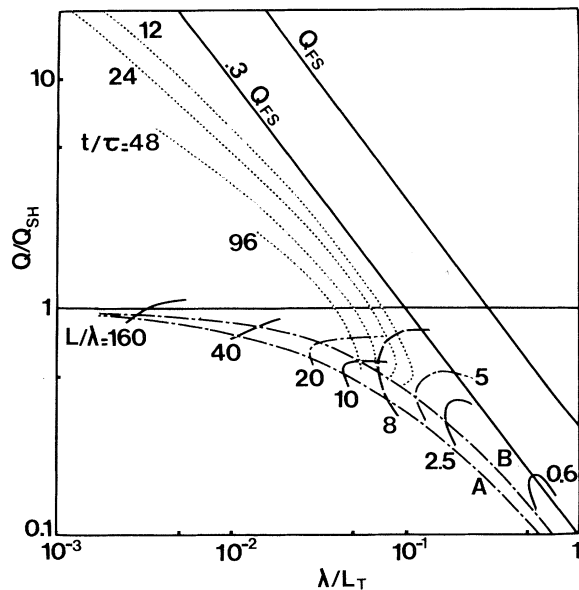


FIG. 1. Reduced-variable plot of the simulation results. For steady-state results, the curves are labeled by the reduced slab length $L/\bar{\lambda}$, where $\bar{\lambda}$ is evaluated at energy $\frac{3}{2}K(T_1 + T_2)/2$. Solid, dash-dotted, and dashed lines, respectively, correspond to temperature ratios $T_1/T_2 = 2, 4,$ and 9 . For transient results (dotted lines, system $L/\bar{\lambda} = 20, T_1/T_2 = 4$), the curves are labeled by the reduced time t/τ . Curves A and B are empirical best fits.

Most simulations used a temperature ratio (T_1/T_2) of 2, but a few used 4 and one used 9. The length of the plasma slab (L) was varied from $0.6\bar{\lambda}$ to $160\bar{\lambda}$, where $\bar{\lambda}$ is the mean free path (mfp) of an electron of energy $\frac{3}{2}K(T_1 + T_2)/2$. Most simulations used six terms in the Legendre polynomial expansion of the distribution function ($N = 5$), but comparisons were made with more ($N = 15$) and fewer ($N = 1$) terms.

As expected, the simulation with a very long slab, $L = 160\bar{\lambda}$, $T_1/T_2 = 2$, gave the Spitzer result to within 3%. On the other hand, a collisionless run was made and gave an upper limit to the heat flow. This required many terms in the angular expansion ($N = 15$) to give the correct value. However, in all collisional cases, including $L = 0.6\bar{\lambda}$, $N = 5$ was entirely adequate (approximately 1% change in Q) and $N = 1$ was found to be sufficient: For $L = 10\bar{\lambda}$, the change in Q was 5%; for $L = 0.6\bar{\lambda}$, Q changed by 20% as compared to the $N = 5$ simulation. This does not imply that the high-order terms (f_2, f_3, \dots) are negligible in magnitude, but that their influence on f_1 (which describes heat flow and current) and f_0 (temperature and density) is small.

Figure 1 summarizes our steady-state results. Each curve corresponds to a different simulation, labeled by its $L/\bar{\lambda}$ and T_1/T_2 values. Each point on each curve is one spatial point. Local values of temperature T , temperature gradient length L_T , and mean free path λ (evaluated at $\frac{3}{2}KT$) are used to calculate the local Spitzer-Härm heat flux Q_{SH} , and hence the ratios Q/Q_{SH} and λ/L_T . Also included in Fig. 1 are four curves

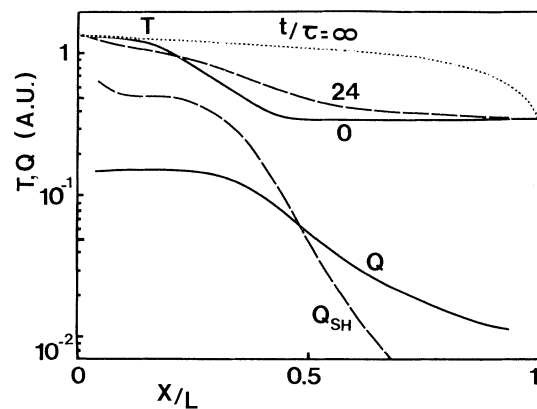


FIG. 2. Profiles for a transient situation. The three upper curves are temperature profiles, at various times t/τ . The two lower curves are profiles of the simulation heat flux Q and of Spitzer's heat flux Q_{SH} at time $t/\tau = 24$.

at different times ($t/\tau = 12, 24, 48, 96$, where τ is the mean collision time), for the non-steady-state simulation ($L/\bar{\lambda} = 20$, $T_1/T_2 = 4$).

The lower Q/Q_{SH} values on each curve correspond to the hottest part of the plasma, and these lie close to curve A,

$$Q_A = [Q_{SH}^{-3/4} + (0.3Q_{FS})^{-3/4}]^{4/3},$$

which was obtained by Khan and Rognlien,⁵ in their $T_1/T_2 = \frac{4}{3}$ simulations. For comparison, curve B is the simple harmonic law $Q_B = [Q_{SH}^{-1} + (0.3Q_{FS}^{-1})]^{-1}$. Our simulations have reached values of Q/Q_{FS} as high as 0.3, in agreement with Refs. 4 and 7, as opposed to only 0.1 in Ref. 6. This is because we have run the code with steeper temperature gradients (higher λ/L_T): compare our Fig. 1 to their Fig. 2.

Whereas curve A describes the hot part of the plasma well, the colder parts lie above it, as a result of nonlocal effects: hot electrons streaming from the hot to the cold region. At steady state, this difference is seen to be higher for larger values of T_1/T_2 . In the transient state, the heat flux in the cold region is seen to exceed the Spitzer-Härm value considerably, again because of hot electrons. This appears more clearly in Fig. 2, where we have plotted temperature profiles, at times $t=0$ and $t=24\tau$, as well as the heat fluxes Q and Q_{SH} at $t=24\tau$. In the hot region,

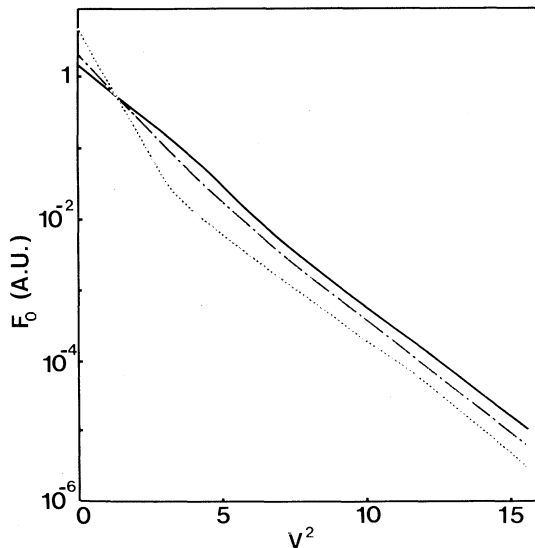


FIG. 3. Isotropic component f_0 vs square velocity v^2 , near the hot wall (solid line), at the center (dash-dotted line), and near the cold wall (dotted line). The slab parameters are $L/\bar{\lambda} = 5$, $T_1/T_2 = 4$. v^2 is in units of $K(T_1 + T_2)/m$.

Q is smaller than Q_{SH} , whereas in the cold region, Q is greater than Q_{SH} but less than Q in the hot region: Q_{SH} diminishes by a factor of 100, but Q diminishes by a factor of 10 only.

The key to the observed heat fluxes is seen in Figs. 3 and 4. In Fig. 3, the plot of the isotropic part of the distribution function f_0 vs v^2 at the center and near each end shows a bi-Maxwellian behavior: a hot component at the hot temperature, whose density diminishes with distance from the hot boundary, and a main component with a bulk temperature which also diminishes from left to right.

In Fig. 4, we compare distribution functions in the center of the simulation region. We plot $f_0 v^5$ and $f_1 v^5$ from the simulation, and $f_{0M} v^5$ and $f_{1M} v^5$ where f_{0M} is the local Maxwellian and f_{1M} is evaluated "à la Spitzer" with use of f_{0M} [i.e., using Eq. (2) with $l=1$, $f_0 \equiv f_{0M}$, and terms $\partial f_1/\partial t$ and $\sim f_2$ neglected]. It is seen that the Maxwellian assumption yields a large f_{1M} , very different from the simulation f_1 . The ratio f_{1M}/f_{0M} is very large at high velocities, while f_1/f_0 remains modest (< 1.5). Even in the steepest gradients ($L/\bar{\lambda} = 0.6$), we have always had $f_1/f_0 < 2$. (Note that for a beam, $f_1/f_0 = 3$; for a semi-isotropic

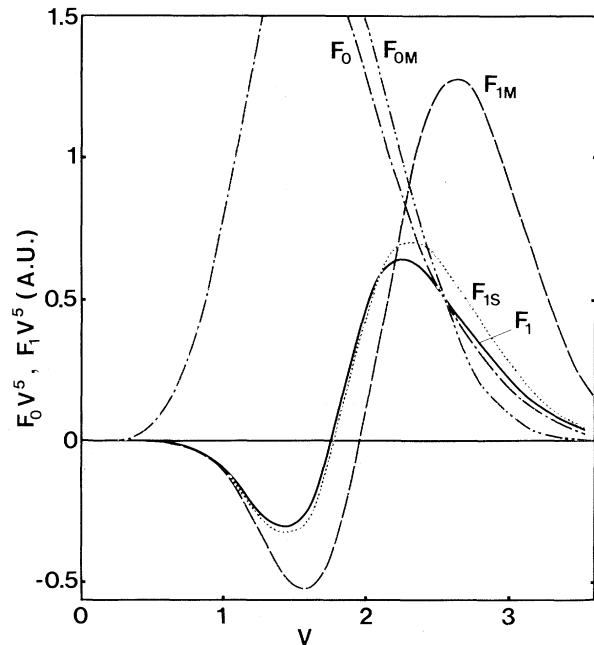


FIG. 4. Comparison of f_0 from the simulation, local Maxwellian f_{0M} , f_1 from the simulation, f_{1S} evaluated à la Spitzer with f_0 from the simulation, and f_{1M} evaluated à la Spitzer with local Maxwellian f_{0M} . All f_0 and f_1 have been multiplied by v^5 .

distribution, $f_1/f_0 = 1.5$.)

The explanation is twofold: In cold regions, f_0 is larger than f_{0M} at high velocities, as a result of the hot tail, and in all cases f_1 is smaller than f_{1M} . To explain this latter result, we have plotted $f_{1S}v^5$ in Fig. 4, with f_{1S} calculated à la Spitzer by using the simulation result for f_0 . f_{1S} is seen to be close to the simulation result f_1 . This is to be expected, because $\partial f_1/\partial t$ is found small and f_2 has a small influence as shown above. A careful examination of the calculation of f_{1M} and f_{1S} shows that the main reason why f_{1S} is smaller than f_{1M} is that the two driving terms $v \partial f_0/\partial x$ and $E \partial f_1/\partial v$ cancel each other out to a higher degree in the former case ($\sim 90\%$) than in the latter ($\sim 50\%$). This is related to the tendency of the energetic part of f_0 to behave like a uniform-temperature, nonuniform-density, Maxwellian distribution, for which

$$v \partial f_0/\partial x \sim \partial f_0/\partial v \sim v \exp(-\frac{1}{2}mv^2/KT_1).$$

These properties are specific to electron transport, and have no equivalence for photons, neutrons, fast ions, etc.

Not shown in Fig. 4 is f_1^* evaluated by the method of Ref. 9: $f_1^* = \min(f_{1M}, f_{0M})$ with E chosen to cancel the current. In hot regions, it would be at least in qualitative agreement with f_1 , but in cold regions f_1^* is much smaller than f_1 .

We thank Dr. C. Moser and Dr. M. Haines, who organized the 1981 CECAM workshop on heat flux which helped to further advance this work. Useful discussions with the participants and Dr. T. W. Johnston are gratefully acknowledged. This research was supported partially by the Natural Sciences and Engineering Council of Canada.

¹W. L. Kruer, Comments Plasma Phys. 5, 69 (1979).

²L. Spitzer and R. Härm, Phys. Rev. 89, 977 (1953).

³D. R. Gray and D. J. Kilkenny, Plasma Phys. 22, 81 (1980).

⁴R. J. Mason, Phys. Rev. Lett. 47, 652 (1981).

⁵S. A. Khan and T. D. Rognlien, Phys. Fluids 24, 1442 (1981).

⁶A. R. Bell, R. G. Evans, and D. J. Nicholas, Phys. Rev. Lett. 46, 243 (1981).

⁷D. J. Bond, Phys. Lett. 88A, 144 (1982).

⁸J. P. Matte and J. Virmont, in Report on the CECAM Workshop on the Flux Limiter and Heat Flow Instabilities, 14 September–2 October 1981, Orsay, France (unpublished).

⁹D. Shvarts, J. Delettrez, R. L. McCrory, and C. P. Verdon, Phys. Rev. Lett. 47, 247 (1981).

¹⁰S. P. Gary, A. G. Sgro, and A. W. De Silva, Phys. Fluids 21, 2103 (1978).

Asymptotic Solutions of the Nonlinear Three-Wave System

M. N. Bussac

Centre de Physique Théorique de l'École Polytechnique, F-91128 Palaiseau Cédex, France

(Received 21 July 1982)

An analytical method is developed for the investigation of the nonlinear state resulting from instability saturation by resonant mode coupling.

PACS numbers: 52.35.Py, 52.35.Ra

An important problem in plasma physics is to determine the nonlinear state from a linear instability. One of the saturation mechanisms of plasma instabilities is the resonant mode coupling of energy in the unstable wave to other waves which are linearly damped. The simplest model of this process is the nonlinear decay of a coherent unstable wave into its subharmonic, which is described by the following system:

$$\begin{aligned} i(dA_0/dt - \gamma_0 A_0) &= A_1^2 \exp(-i\Delta\omega t), \\ i(dA_1/dt + \gamma_1 A_1) &= A_0 A_1^* \exp(+i\Delta\omega t), \end{aligned} \quad (1)$$

where $A_j = |A_j| \exp(i\varphi_j)$, $j=0,1$, are time-dependent complex wave amplitudes, A_j^* is the complex conjugate of A_j , γ_0 is the growth rate of the high-frequency wave A_0 and γ_1 the damping rate of the low-frequency wave A_1 , $\Delta\omega$ is the mismatch in the frequency resonance, and amplitudes have been normalized so that the coefficients of nonlinear terms are 1. Numerical investigations of this system have shown that nonlinear saturation of the instability occurs if $\Delta\omega \neq 0$ and for γ_1/γ_0 large enough.^{1,2} If so, the time behavior of the wave amplitudes and phases is either periodic